AGU PUBLICATIONS

JGR

Journal of Geophysical Research: Biogeosciences

RESEARCH ARTICLE
10.1002/2017JG004100

Key Points:
- An isopycnal mixing model revealed the influence of the Kuroshio Current and mesoscale eddies on organic matter in the South China Sea
- The Kuroshio intrusion modulated humic-like fluorescence in the upper South China Sea; protein-like fluorescence was produced in situ
- Export of excess dissolved organic matter in South China Sea intermediate water may deliver refractory carbon to the deep Pacific Ocean

Supporting Information:
- Supporting Information S1
- Data Set S1

Correspondence to:
W. Guo,
wdguo@xmu.edu.cn

Citation:
Wang, C., Guo, W., Li, Y., Stubbins, A., Li, Y., Song, G., … Cheng, Y. (2017). Hydrological and biogeochemical controls on absorption and fluorescence of dissolved organic matter in the northern South China Sea. *Journal of Geophysical Research: Biogeosciences*, *122*, 3405–3418. https://doi.org/10.1002/2017JG004100

Received 8 AUG 2017
Accepted 30 NOV 2017
Accepted article online 6 DEC 2017
Published online 29 DEC 2017

Hydrological and Biogeochemical Controls on Absorption and Fluorescence of Dissolved Organic Matter in the Northern South China Sea

Chao Wang[1], Weidong Guo[1,2], Yan Li[3], Aron Stubbins[4], Yizhen Li[5], Guodong Song[6], Lei Wang[2,3], and Yuanyue Cheng[7]

[1]State Key Laboratory of Marine Environmental Science, College of Ocean and Earth Sciences, Xiamen University, Xiamen, China, [2]Key Laboratory of Coastal and Wetland Ecosystems, Ministry of Education, Xiamen University, Xiamen, China, [3]Fujian Provincial Key Laboratory for Coastal Ecology and Environmental Studies, Xiamen University, Xiamen, China, [4]Skidaway Institute of Oceanography, Department of Marine Sciences, University of Georgia, Savannah, GA, USA, [5]Department of Applied Ocean Physics and Engineering, Woods Hole Oceanographic Institution, Woods Hole, MA, USA, [6]Key Laboratory of Marine Chemistry Theory and Technology, Ministry of Education, Ocean University of China, Qingdao, China, [7]South China Sea Institute of Oceanology, Chinese Academy of Sciences, Guangzhou, China

Abstract The Kuroshio intrusion from the West Philippine Sea (WPS) and mesoscale eddies are important hydrological features in the northern South China Sea (SCS). In this study, absorption and fluorescence of dissolved organic matter (CDOM and FDOM) were determined to assess the impact of these hydrological features on DOM dynamics in the SCS. DOM in the upper 100 m of the northern SCS had higher absorption, fluorescence, and degree of humification than in the Kuroshio Current of the WPS. The results of an isopycnal mixing model showed that CDOM and humic-like FDOM inventories in the upper 100 m of the SCS were modulated by the Kuroshio intrusion. However, protein-like FDOM was influenced by in situ processes. This basic trend was modified by mesoscale eddies, three of which were encountered during the fieldwork (one warm eddy and two cold eddies). DOM optical properties inside the warm eddy resembled those of DOM in the WPS, indicating that warm eddies could derive from the Kuroshio Current through Luzon Strait. DOM at the center of cold eddies was enriched in humic-like fluorescence and had lower spectral slopes than in eddy-free waters, suggesting inputs of humic-rich DOM from upwelling and enhanced productivity inside the eddy. Excess CDOM and FDOM in northern SCS intermediate water led to export to the Pacific Ocean interior, potentially delivering refractory carbon to the deep ocean. This study demonstrated that DOM optical properties are promising tools to study active marginal sea-open ocean interactions.

1. Introduction

Chromophoric dissolved organic matter (CDOM), the fraction of dissolved organic matter (DOM) that interacts with solar radiation, is ubiquitous in natural waters, including marginal seas and the open ocean (Guo et al., 2014; Jørgensen et al., 2011; Nelson et al., 2010). CDOM is important owing to its involvement in photochemistry and photobiology, its utility as a tracer of ocean circulation, its role in the biogeochemistry of carbon, trace elements and gases, and its pertinence to ocean optics and remote sensing (Siegel et al., 2002; Swan et al., 2009). CDOM in marginal seas and open oceans is mainly produced in situ by biological production and removed by photochemical degradation and microbial consumption (Mopper, Kieber, & Stubbins, 2015; Nelson & Siegel, 2013; Yamashita & Tanoue, 2008). The contribution of terrestrial CDOM is limited owing to rapid removal processes (flocculation and photolysis) (Coble, 2007). The distribution patterns of CDOM are also regulated by various physical processes in marine environments (e.g., water mass mixing, upwelling, and mesoscale eddies) (Kowalczuk et al., 2013; Nelson et al., 2007; Zhang et al., 2009).

The optical properties of DOM have been widely applied to describe the dynamics of its biogeochemistry in the global ocean (Nelson & Siegel, 2013, and references therein). Absorption coefficients at certain wavelengths have been used to quantify the abundance of CDOM, while the spectral slopes between ranges of wavelengths provide further insights into the chemistry (e.g., molecular weight), source, and processing of DOM (Helms et al., 2008). A small fraction of CDOM is able to emit fluorescence after absorbing light and is termed fluorescent DOM (FDOM). Like absorption, fluorescence intensities at or across certain excitation: emission wavelength pairs are used to quantify FDOM, whereas ratios of intensities between wavelength pairs are used to describe DOM composition or quality. FDOM provide further information about the

quality, source, and processing of DOM. Complex excitation-emission fluorescence spectra can be decomposed into independent fluorescence components by parallel factor analysis (EEM-PARAFAC) (Guo et al., 2014; Stedmon & Bro, 2008; Stedmon, Markager, & Bro, 2003). Variations in the resultant fluorescent components can then be applied to describe changes of FDOM resulting from mixing, biological degradation, biological productivity, and photochemistry (Helms et al., 2013; Tanaka et al., 2014). For instance, two humic-like fluorescent components (peak A-C and peak M) are commonly identified in ocean waters (Jørgensen et al., 2011). The ratio of M:C can be a good indicator of photochemical and microbial degradation (Hansen et al., 2016; Helms et al., 2013; Moran, Sheldon, & Zepp, 2000). Although the optical properties of DOM have been reported for much of the world's oceans, little is known about the dynamics of CDOM and FDOM in tropical oligotrophic marginal seas (Coble, Del Castillo, & Avril, 1998; Fichot & Benner, 2011; Lorenzoni et al., 2011; Nelson, Siegel, & Michaels, 1998).

The South China Sea (SCS) is the largest tropical marginal sea in the Pacific Ocean (Chen et al., 2001; Wong et al., 2007) and plays an important role in the global carbon cycle as a recognized source of atmospheric CO_2 (Chen et al., 2001; Dai et al., 2009, 2013; Wyrtki, 1961). Although many rivers (e.g., Pearl, Mekong, and Red Rivers) carry an abundance of terrestrial materials into the SCS, surface water in the SCS basin is overall oligotrophic due to the effective isolation of surface circulation gyres (Wong et al., 2007). At the basin scale, surface circulation reverses seasonally under the persistent influence of monsoonal winds, resulting in a basin-wide cyclonic circulation gyre during the northeast winter monsoon season and an anticyclonic circulation gyre around the southern half of the SCS during the southwest summer monsoon season (Wong et al., 2007). In the upper layer ($<$500 m), the northern SCS is influenced by the intrusion of the extremely oligotrophic Kuroshio Current, especially in winter and spring (Qu, Mitsudera, & Yamagata, 2000). Dissolved organic carbon (DOC) in the upper layer of the West Philippine Sea (WPS) is higher than in the northern SCS (Wu et al., 2015). At depths greater than 1,500 m, entrainment of various water masses from the adjacent Pacific Ocean facilitates deep ocean exchange (Tian et al., 2006). Eastward outflow at intermediate depths (500–1,500 m) to the WPS is the largest outflow of SCS water (Wong et al., 2007). The net outflow of DOC-enriched SCS intermediate water through Luzon Strait exports 54.7 ± 15.0 Tg C yr^{-1} to the WPS (Dai et al., 2009; Wu et al., 2015). This DOC export has implications for the production, degradation, and sequestration of organic carbon in the SCS and WPS, as well in the Pacific Ocean at large. However, the characteristics of CDOM and FDOM in the SCS and WPS remain unclear, limiting our understanding of the impact of the Kuroshio intrusion on DOM dynamics in the upper northern SCS, and the importance of CDOM and FDOM export from the SCS to the Pacific Ocean, and its role in the global ocean carbon reservoir.

Mesoscale eddies are ubiquitous features throughout the SCS and WPS and play an important role in regulating regional biogeochemical processes (Li, Nowlin, & Jilan, 1998; McGillicuddy Jr. et al., 1998, 2016; Xiu et al., 2010). Mesoscale eddies influence nutrient supply to the euphotic layer, which changes phytoplankton productivity and particle export to the deep sea (Chen et al., 2007; Lin et al., 2010). There are some studies in the SCS concerning the biogeochemical impacts due to mesoscale eddies (Chen et al., 2015; Huang et al., 2010; Xiu & Chai, 2011; Zhou et al., 2013). However, only one study concentrates on the response of CDOM and FDOM dynamics to cold eddy (Zhang et al., 2009).

We present the quantitative (i.e., absorption coefficients and fluorescence intensities) and qualitative (i.e., spectral slope and fluorescence indices) parameters of CDOM and FDOM in the northern SCS and WPS. Our aims are to determine (1) the distribution patterns of CDOM and FDOM in the northern SCS and WPS, (2) the impact of the Kuroshio intrusion on the CDOM and FDOM dynamics in the upper water column of the northern SCS, (3) how mesoscale eddies influence CDOM and FDOM in the northern SCS, and (4) the in situ production of CDOM and FDOM in the intermediate water and their contributions to the export of DOC from the intermediate water masses of the SCS to the WPS.

2. Materials and Methods

2.1. Sample Collection, Pretreatment, and Measurement of Auxiliary Parameters

Water samples were collected at 26 stations from the surface down to 1,500 m in the northern SCS and the adjacent Kuroshio region of the WPS during April–May 2014 (Figure 1). Twelve casts with a conductivity-temperature-depth (CTD)/carousel sampling system equipped with 5 L Niskin bottles were used to obtain vertical profiles. Vertical profiles of temperature and salinity were recorded with a calibrated SeaBird

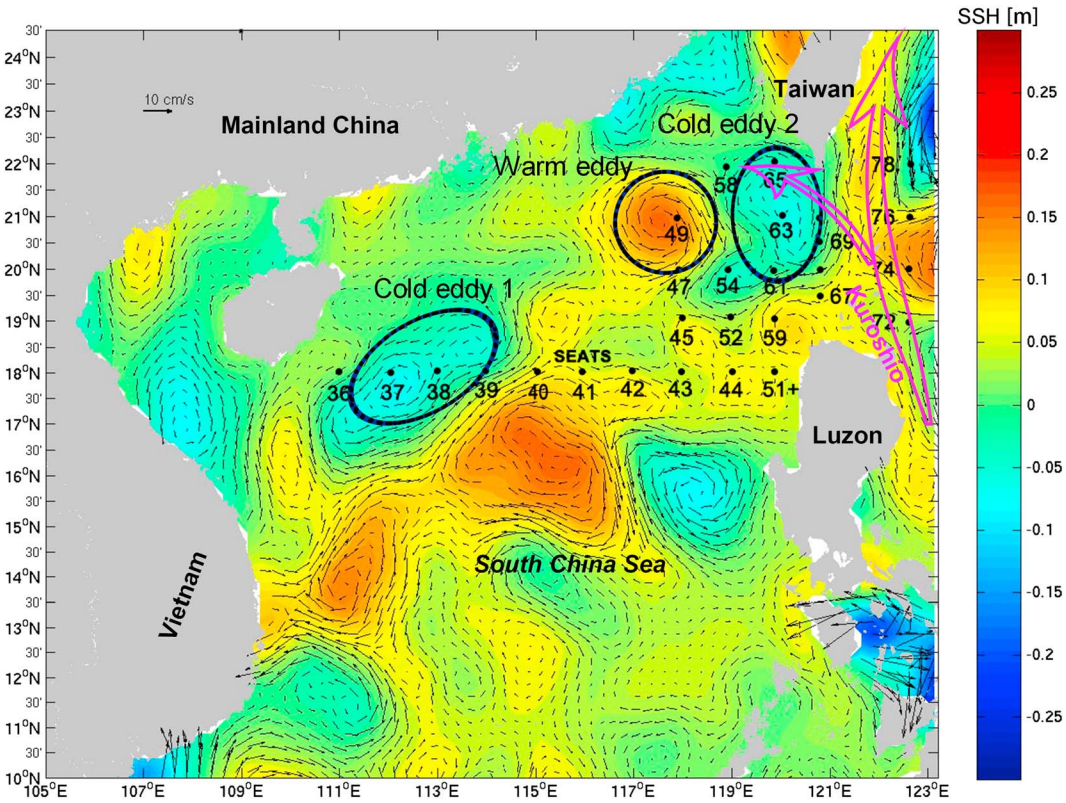

Figure 1. Sampling stations in the northern South China Sea (SCS) and the adjacent Kuroshio Current of the West Philippine Sea (WPS) superimposed with the AVISO sea surface height (SSH) and the derived surface geostrophic currents during a March–April 2014 ship survey. The Kuroshio Current and its intrusion pathways into the northern SCS are shown (in pink vectors). Cold eddies 1 and 2 and warm eddy were highlighted by dark blue ellipses. SEATS: SouthEast Asian Time-series Study (Wong et al., 2007).

CTD system (SeaBird 911 plus, USA). Dissolved oxygen was measured on board using the Winkler titration method (Carpenter, 1965). Apparent oxygen utilization (AOU) was computed from temperature, salinity, and oxygen using algorithms in Ocean Data View (v 4.5.4). For total Chlorophyll *a* (Chl *a*) analysis, 3 to 4 L samples were collected from the upper 200 m and filtered onto GF/F filters (nominal pore size ~ 0.7 μm) under a gentle vacuum of <150 mm Hg. The filters were stored in liquid nitrogen until analysis. Chl *a* concentration was measured using high-performance liquid chromatography following the protocol of Huang et al. (2010). Samples for CDOM and FDOM analysis were filtered immediately through precombusted (500°C, 5 h) GF/F filters (Whatman, UK) and stored in precombusted (500°C, 5 h) amber glass bottles, which were kept frozen on board. Freezing filtered water samples at −20°C is a commonly used method for DOM analysis, and a number of marine DOM studies show the minimal effect of freeze/thaw on DOM optical properties (Coble et al., 1998; Conmy et al., 2009; Spencer & Coble, 2014; Yamashita et al., 2010). CDOM and FDOM analyses were finished within 1 month after cruise.

2.2. Absorption Spectroscopy Analysis

CDOM absorption spectra were determined using a liquid wavelength capillary cell system (WPI Inc., U.S.A) using published methods (D'Sa et al., 1999; Miller et al., 2002). Water samples were uniformly injected into the capillary cell through a teflon tube (precleaned with 1 M HCl) using a peristaltic pump (Baoding Longer Inc., China) at a pump speed of 1.5 mL min^{-1}. Incident light was provided by a balanced deuterium halogen source (DH-2000-BAL, Ocean Optics Inc., U.S.A) and introduced into the capillary cell via an optical fiber (QP-400-2-UV/Vis, Ocean Optics Inc., U.S.A; Stubbins et al., 2006). The light at the export of the capillary cell was collected by another optical fiber connected to a diode array spectrophotometer (USB-4000-UV–Vis, Ocean Optics Inc., U.S.A). Absorption spectra were recorded between 250 and 800 nm at 0.2 nm using the SpectraSuite software.

Milli-Q water was used as the reference spectrum, and the dark current spectrum was deducted. Each sample was measured three times to ensure repeatability, and Milli-Q water was measured every five samples to provide blanks to correct any baseline drift. To correct the difference of refractive index between seawater and pure water, an artificial seawater medium with approximately the same refractive index was prepared with NaCl (precombusted at 450°C for 10 h to remove possible organic moieties). Baseline drift was further corrected by subtracting the absorption at 700 nm from the entire spectrum. Fastidious elimination of microbubbles in the capillary cells was employed as it can greatly reduce baseline offsets and improve CDOM spectral slope precision (Floge et al., 2009).

CDOM Naperian absorption coefficients ($a_{CDOM}(\lambda)$) were calculated using the following equation:

$$a_{CDOM}(\lambda) = A(\lambda)/L \quad (1)$$

where $A(\lambda)$ is the absorbance (unitless) measured by the spectrophotometer at wavelength λ (nm) and L (m) is the effective optical path length of the liquid wavelength capillary cell (0.9948 m in this study). The spectral slope over the range 275 to 295 nm ($S_{275-295}$) was calculated by linear regression of the natural log-transformed absorption spectra (Helms et al., 2008).

2.3. Fluorescence Measurements and PARAFAC Modeling Analysis

Fluorescence measurements were performed using a 1 cm quartz cuvette and a Varian Cary Eclipse spectrofluorometer. Emission spectra were scanned every 2 nm at wavelengths from 280 to 600 nm, with excitation wavelengths ranging from 240 to 450 nm at 5 nm intervals. Slit widths were 10 nm for both excitation (ex) and emission (em). The EEM spectra (EEMs) were Raman normalized and blank corrected using Raman normalized Milli-Q water EEMs scanned on the same day (Guo et al., 2011, 2014). Inner filter corrections were not applied to these samples because of the low absorbance of our open ocean samples (Nelson et al., 2007). EEMs were decomposed into components using parallel factor analysis (PARAFAC), with MATLAB 2012 and the DOMFluor toolbox (Stedmon et al., 2003; Stedmon & Bro, 2008). The maximum fluorescence (F_{max}) intensity of PARAFAC components are reported in Raman Units (RU) (Lawaetz & Stedmon, 2009). Three fluorescence parameters were used to account for the DOM composition and characteristics (humification index (HIX), biological index (BIX), and M:C). The humification index (HIX) is calculated as the integrated emission spectra at 435–480 nm divided by this emission area plus at 300–345 nm when excited at 254 nm (Ohno, 2002). Higher values indicate an increasing degree of humification. The BIX is the ratio of fluorescence intensity emitted at em 380 nm divided by the intensity at 430 nm, obtained at ex 310 nm, which varies with the contribution of recently produced DOM in aquatic ecosystems (Coble et al., 2014; Huguet et al., 2009). M:C is defined as the ratio of peak M and peak C intensity, which is an indication of the amount of blue-shifted fluorescence in a sample (Hansen et al., 2016; Helms et al., 2013).

3. Results

3.1. Hydrologic Background and Eddy Characterization

The distributions of hydrologic parameters in the northern SCS and the adjacent Kuroshio region of the WPS during our cruise were similar to previous results (Du et al., 2013; Wu et al., 2015, Figure 2). Kuroshio water had higher potential temperature (θ) and salinity (S) than the SCS water along the isopycnal layer in the upper water column at a potential density of $<$1025.7 kg m^{-3}. However, in deeper waters ($>$200 m) Kuroshio water had lower potential temperature and salinity than the SCS. AOU showed no significant trends in the mixed layer (~25 m).

Below the mixed layer, AOU decreased along the isopycnal layer from the northern SCS to the WPS. Almost all θ-S points fell between the θ-S lines of the SCS and WPS end-members, indicating water exchange between the northern SCS and WPS. The vertical profiles of θ, S, Chl *a*, and DO for a typical station in both the SCS and WPS are shown in Figure S1 in the supporting information. The maximum Chl *a* occurred at a greater depth and lower concentration (0.1 μg L^{-1}) in the WPS (~100 m) than in the SCS (depth = 50 m; concentration = 0.25 μg L^{-1}).

One warm eddy (ACE) and two cold eddies (CE1 and CE2) were identified from sea surface height anomaly data and surface geostrophic currents confirmed their anticyclonic and cyclonic characteristics, respectively (Figure 1). The centers of CE1 and CE2 were located at ~18.0°N:113.5°E (close to station 38) and

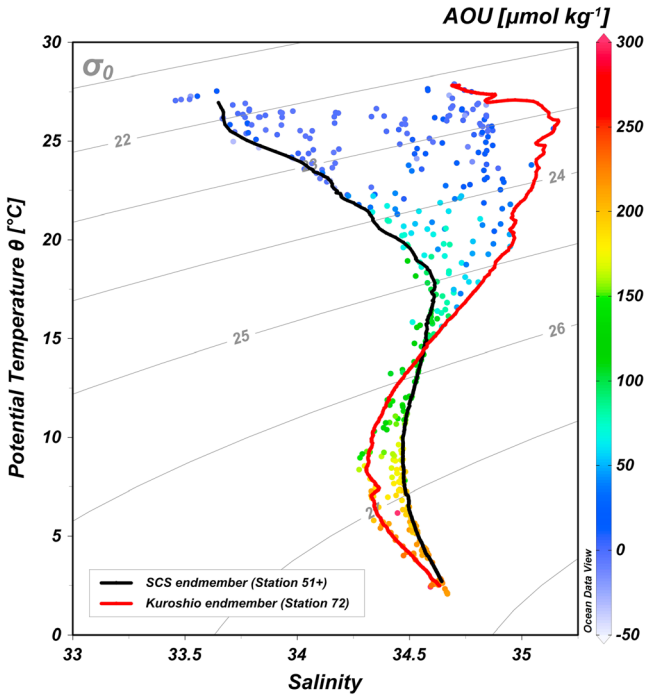

Figure 2. Potential temperature (θ) versus salinity (S) plot for the sampling stations superimposed with AOU (color gradation). Data of the Kuroshio (red line) and SCS (black line) were obtained from the CTD profile data of stations 51^{+} and 72.

~21.3°N:119.5°E (close to station 63), respectively (Figure 1). The core of the warm eddy was located at ~21.2°N:117.8°E (close to station 49). The warm eddy was stronger than the cold eddies during our cruise, with the maximum sea level anomaly for the warm eddy of +18 cm, compared to −12 cm for cold eddies 1 and 2.

3.2. PARAFAC Components

Five fluorescent components were identified using EEMs-PARAFAC, including two humic-like (C1 and C2) and three protein-like (C3, C4, and C5) components (Figure S2). C1 displayed two excitation maxima at 250 and 365 nm and one emission maxima at 456 nm. Similar fluorescence signatures are initially categorized as representing a mixture of terrestrial humic-like fluorescence peaks A and C (Coble, 1996) but have also been widely observed in oceanic waters (Catalá et al., 2015; Guéguen et al., 2014; Jørgensen et al., 2011; Kowalczuk et al., 2013; Loginova, Thomsen, & Engel, 2016; Yamashita et al., 2010). C2 had excitation/emission maxima at 250, 330/388 nm, consistent with marine humic-like fluorescence (peak M; Coble, 1996), which has been characterized as representing microbially altered DOM (Stedmon & Markager, 2005; Yamashita et al., 2007). C3, C4, and C5 are characterized as amino acid-like DOM, displaying narrower emission spectra with maxima below 350 nm (Jørgensen et al., 2011). C3 had an excitation/emission maximum at 270/296 nm, similar to tyrosine-like peak B (Coble, 1996). C4 had an excitation/emission maximum at 275/344 nm, representing tryptophan-like peak T (Coble, 1996, 2007). C5 had an excitation/emission maximum at 250/320 nm, similar to phenylalanine-like fluorescence (Jørgensen et al., 2011). Although tyrosine-like C3 and phenylalanine-like C5 are often present in marine DOM, their fluorescences are difficult to quantify precisely because of energy transfer to tryptophan and tyrosine and quenching by neighboring chemical groups in the same protein (Lakowicz, 2006). Therefore, tryptophan-like C4 was selected to represent the labile protein-like component. Similar PARAFAC results are reported in previous FDOM studies in marginal seas and the open ocean (Catalá et al., 2015; Jørgensen et al., 2011; Kowalczuk et al., 2013; Loginova et al., 2016; Yamashita et al., 2010).

3.3. Chromophoric and Fluorescent Dissolved Organic Matter Distribution in the Northern South China Sea and Adjacent Kuroshio Region of the West Philippine Sea

Humic-like C1 and C2 fluorescence intensities and a_{CDOM} (350) were lowest in surface waters, increasing with depth to approximately constant levels in intermediate and deep waters of the northern SCS and Kuroshio region of the WPS (Figure 3). By contrast, protein-like C4 fluorescence intensity was highest in surface waters, decreasing to approximately constant low levels below ~500 m. Similar CDOM and FDOM profiles have been observed in marginal seas, including the Arabian Sea (Coble et al., 1998), Okhotsk Sea (Yamashita et al., 2010), and Japan Sea (Tanaka et al., 2014), as well as in the open ocean (Jørgensen et al., 2011). Vertical gradients in C1 and C2 had significant differences in the northern SCS (t test, $p < 0.01$). C2 had a steeper vertical gradient (~1.8×10^{-5} RU m^{-1}) than C1 (~8.8×10^{-6} RU m^{-1}) in the upper 200 m of the water column. The levels of C1, C2, C4, and a_{CDOM} (350) from the surface to 1,500 m in the Kuroshio Current of the WPS ranged from 0.0009 to 0.013, 0.0004 to 0.009, 0.0011 to 0.0078 RU, and 0.07 to 0.20 m^{-1}, respectively. They were significantly lower than the values in the northern SCS (t test, $p < 0.01$).

HIX showed a positive linear correlation with the fluorescence intensities of humic-like components ($I_{humic\text{-}like}$, sum of C1 and C2) ($R^2 = 0.72$, $p < 0.001$, $n = 295$; Figure S3a). BIX represents the contribution of recently produced DOM and showed a negative linear correlation with $I_{humic\text{-}like}$ and HIX ($R^2 = 0.67$, $p < 0.001$, n = 295; Figure S3b). $S_{275-295}$ showed significant negative correlation with a_{CDOM} (350) in the northern SCS and WPS ($R^2 = 0.43$, $p < 0.001$, $n = 286$; Figure S3c). Surface water had the lowest HIX values (~0.3), the highest BIX values (~1.6), and an $S_{275-295}$ value of 0.05 nm^{-1} (Figure 3). HIX gradually increased with depth, while BIX and $S_{275-295}$ decreased with depth and they were all approximately constant below ~400 m (Figure 3). The

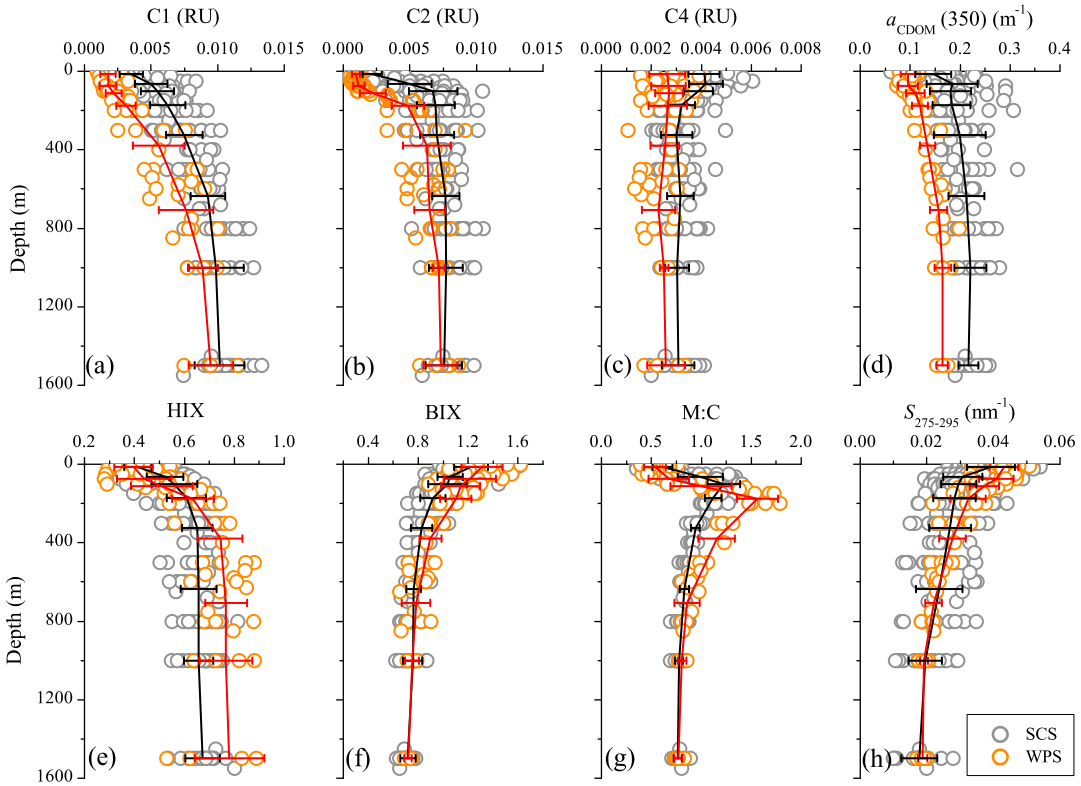

Figure 3. Vertical profiles of C1, C2, C4, a_{CDOM} (350), HIX, BIX, M:C, and $S_{275–295}$ in the northern SCS (gray circles) and the adjacent Kuroshio Current of the WPS (orange circles). The black and dark orange lines display the average values calculated from eight depths or depth intervals (0–50; 50–100; 100; 100–200; 200–500; 500–1,000; 1,000; and 1,450–1,550 m) in the northern SCS and adjacent Kuroshio region. The error bars represent standard deviations.

highest HIX (~0.8) and the lowest BIX (~0.8) and $S_{275–295}$ (~0.02 nm^{-1}) were observed in the deep layer (1,500 m; Figure 3). The ratio of humic-like C2 and C1 (C2:C1, i.e., M:C) was lowest in the surface waters, increased rapidly with depth in the euphotic layer, and then reached a maximum at the bottom of the euphotic layer (~100 m; Figure 3g). Subsequently, M:C decreased slightly with depth and showed approximately constant values in water below 1,000 m (~0.77; Figure 3g).

Vertical variation trend of spectral indices with depth in the Kuroshio Current of the WPS were similar to those in the northern SCS. However, the euphotic layer of the WPS had lower HIX, higher BIX, and higher $S_{275–295}$ values than the SCS, suggesting lower relative levels of humic-like substances in the WPS. In addition, higher HIX values were found at greater depth in the WPS (>400 m), while there were no obvious differences of BIX and $S_{275–295}$ between the northern SCS and the WPS in the deep water. M:C had lower values in the euphotic layer and a greater depth of the maximum (~150 m) in the WPS than the northern SCS.

4. Discussion

4.1. Impact of the Kuroshio Intrusion on the Chromophoric Dissolved Organic Matter Dynamics in the Euphotic Layer of the Northern South China Sea

As compared to the WPS, the euphotic layer of the northern SCS had higher CDOM and FDOM levels (Figures 3a–4d), but lower dissolved organic carbon (DOC) concentration (Wu et al., 2015). It was assumed that the lower availability of nutrients limited the growth of bacteria and resulted in the accumulation of DOC in the upper layer of the WPS (Wu et al., 2015). Kuroshio water was depleted in humic-like optical signatures (Figures 3a and 3b) and exhibited steeper spectral slopes (Figure 3c) than samples from the SCS. A depletion in humic-like fluorescence and steep spectral slopes have been observed in the sunlit surface gyres of the open ocean (Jørgensen et al., 2011; Kitidis et al., 2006) and are consistent with highly photobleached DOM (Helms et al., 2013, 2008).

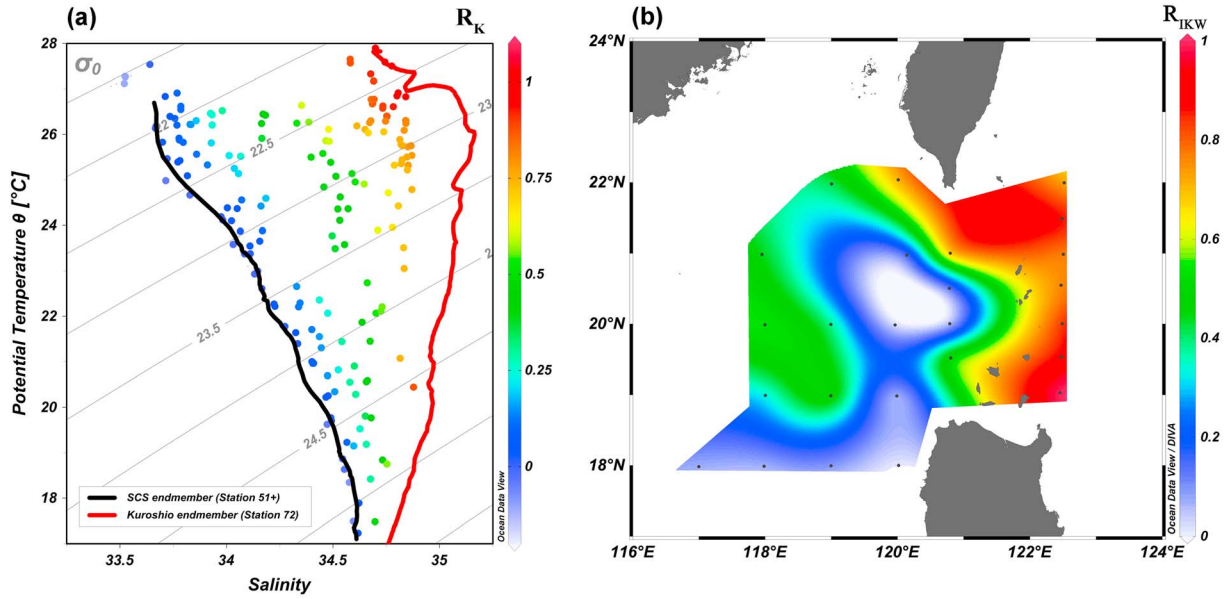

Figure 4. θ-S diagram in the upper 100 m of the water column for the sampling stations in the northern SCS and adjacent Kuroshio region of the WPS superimposed with the (a) isopycnal mixing model-derived Kuroshio water fraction (R_K) and (b) station-integrated Kuroshio water fraction (R_{IKW}) (the black line represents SCS end-member collected at station 51$^+$; the red line represents Kuroshio end-member collected at station 72; the gray lines represent isopycnic lines).

Kuroshio water had lower levels of tryptophan-like (C4) fluorescence but higher C4 as a % of the total fluorescence compared with the upper water column (0–100 m) in the northern SCS. Tryptophan-like fluorescence is associated with primary production in the open ocean (Jørgensen et al., 2011). Therefore, the low levels of tryptophan-like fluorescence in the Kuroshio water are likely a result of the low primary productivity and bacterial abundance in these waters (Du et al., 2013). The CDOM, FDOM, and nitrate plus nitrite (NO_3^- + NO_2^-) inventories in the upper 100 m of the SCS end-member were higher than in the Kuroshio end-member, while the DOC inventory was higher in the Kuroshio end-member than in the SCS end-member (Table 1). Therefore, the intrusion of Kuroshio water into the SCS would likely result in a dilution of CDOM, FDOM, and nitrate plus nitrite, while enriching SCS waters with DOC.

An isopycnal mixing model was adopted to quantify the impact of the Kuroshio intrusion on CDOM and FDOM in the upper water column (~100 m) of the northern SCS (Du et al., 2013). The isopycnal mixing rate of DOC in the SCS was estimated to be 6.0×10^{-3} mmol m^{-2} s^{-1}, which was 3 orders of magnitude larger than the diapycnal mixing rate of ~1.0×10^{-6} mmol m^{-2} s^{-1} in the upper 100 m (Wu et al., 2015). This suggests that diapycnal mixing was negligible and that isopycnal mixing controlled the diffusive transport of CDOM and FDOM in the upper northern SCS. For any in situ observed water parcel represented by a point in the θ-S plot (Figure 2), the fractional contributions of Kuroshio and SCS water can be derived by adopting the conservative along-isopycnal mixing law of potential temperature or salinity (equations (2) and (3)).

$$R_S + R_K = 1 \tag{2}$$

$$R_S\,\theta_S + R_K\,\theta_K = \theta \text{ or } R_S\,S_S + R_K\,S_K = S \tag{3}$$

Table 1
Integrated Fluorophore, Chromophore, DOC, and Nutrient Inventories in the Upper 100 m of the SCS and Kuroshio End-Members

	Fluorophore			Chromophore	DOC[a]	NO_3^- + NO_2^-[b]
End-Member	C1 m·RU	C2 m·RU	C4 m·RU	a_{CDOM} (350)	mol m^{-2}	mmol m^{-2}
SCS	0.498	0.453	0.447	18.7	~6.5	~250
Kuroshio	0.134	0.090	0.281	9.2	~7.5	~5
Δ	−73%	−80%	−37%	−51%	15%	−98%

Note. Water mass end-members were identified from θ-S plot (Figure 2). DOC: dissolved organic matter; NO_3^- + NO_2^-: nitrate plus nitrite.
[a]Data from Wu et al. (2015). [b]Data from Du et al. (2013).

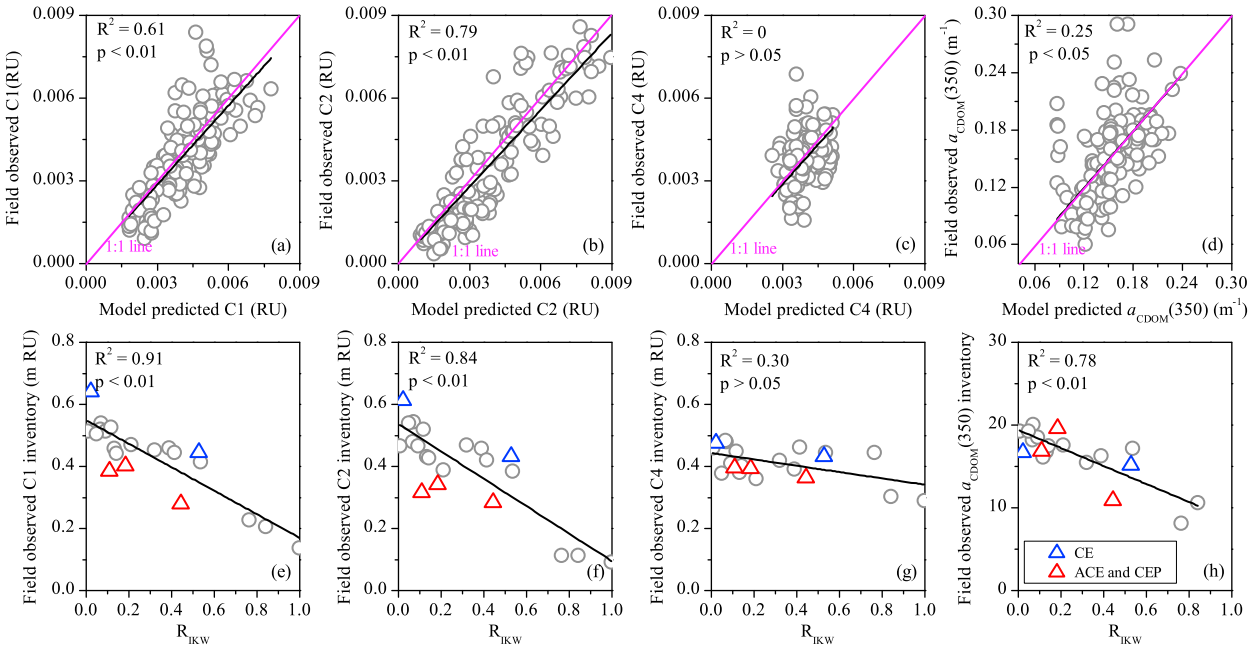

Figure 5. (a–d) Field observed FDOM and CDOM levels versus the model prediction in the upper 100 m of the northern SCS and (e–h) the relationships between the field observed FDOM and CDOM inventories and the station-integrated Kuroshio water proportion (R_{IKW}) (the pink line is the 1:1 line; the black line is the zero intercept linear regression). CE: cold eddy; ACE: warm eddy; CEP: the edges of cold eddy.

Here the Kuroshio water fraction is denoted as R_K, and R_S stands for the SCS water fraction. The θ_S, θ_K and S_S, S_K are the end-member values of potential temperature and salinity for the SCS and Kuroshio water proper, respectively. Salinity was adopted for R_K and R_S calculation in the upper 60 m of the water column due to the fact that temperature in the upper ocean is significantly affected by diurnal and seasonal variation in solar radiation (Tseng et al., 2007). The θ was used for model prediction in deeper water as it provides higher sensitivity than salinity (Figure 2). The Kuroshio water fraction (R_K) for a given station was integrated over the upper 100 m to represent the station-integrated Kuroshio water fraction (R_{IKW}).

The model-derived results showed Kuroshio intrusion in spring, with high R_{IKW} values reaching (~0.4) southwest of Taiwan Island, and lower R_{IKW} values (<0.2) at lower latitudes (≤18°N; Figure 4), in conformity with the cyclonic circulation of the gyre around the SCS in early spring (Chao, Shaw, & Wang, 1995; Wong et al., 2007; Xue et al., 2004). The model-derived Kuroshio water fraction was even lower ($R_{IKW} < 0.1$) in the central Luzon Strait, which was observed as a cold eddy during the cruise period.

Abnormally low seawater temperature inside the cold eddy caused by upwelling could lead to negative deviations of R_K and R_{IKW} according to the model formula (equations (2) and (3)). Thus, cold eddies were excluded when using an isopycnal mixing model to quantify the Kuroshio water fraction. Model-predicted FDOM (C1, C2, and C4) and CDOM (a_{CDOM} (350)) levels and station-integrated inventories in the upper 100 m were calculated based on the fraction of Kuroshio and SCS water along the isopycnal layer and the field observed CDOM and FDOM levels of the two end-members (Figure 5). The model-predicted humic-like FDOM (C1 and C2) agreed well with the field measurements, indicating that isopycnal mixing explained 61% of the variation in C1 and 79% in C2 within the upper 100 m of the northern SCS under a 95% confidence interval (Figures 5a and 5b). However, isopycnal mixing could not explain the variation of the tryptophan-like (C4) component in the upper 100 m of the northern SCS ($R^2 \approx 0$), indicating that other processes (such as in situ biological production or utilization) controlled the distribution of C4 (Figure 5c). Predicted a_{CDOM} (350) showed weak but significant correlation with the field observed a_{CDOM} (350), with a coefficient of determination of 0.25, which fell between the humic-like (C1 and C2) and protein-like (C4) fluorescence signatures (Figure 5d). This suggests that CDOM absorbance is influenced by both mixing and other processes. These additional processes likely include the microbial production, microbial utilization, and photochemical bleaching of CDOM. The field observed humic-like C1, C2, and CDOM inventories in the upper 100 m water column were overall negatively correlated with the station-integrated Kuroshio water proportion (R_{IKW}),

Table 2
Integral Average Values of Physical, Chemical, and Biological Parameters Inside and Outside the Cold Eddies in the Upper 100 m of Northern SCS

	CE1 (Stn. 39)	CEP1 (Stn. 40)	CE2 (Stn. 63)	CEP2 (Stn. 54, 65)
θ (°C)	22.28	23.659	22.022	23.98
Salinity	34.08	33.977	34.129	34.59
σ_0 (kg m^{-3})	23.21	22.951	23.526	23.31
C1 (RU)	0.0044	0.0038	0.0053	0.0037
C2 (RU)	0.0043	0.0031	0.0052	0.0037
C4 (RU)	0.0040	0.0039	0.0045	0.0038
BIX	1.05	1.15	1.07	1.16
HIX	0.46	0.43	0.54	0.49
M:C	0.79	0.72	0.91	0.87
$a_{CDOM}(350)$ (m^{-1})	0.241	0.186	0.161	0.136
$S_{275-295}$ (nm^{-1})	0.0256	0.0258	0.0356	0.0412
DCML (m)	50	75	50	75
Chl a_{max} (μg/L)	0.475	0.378	0.331	0.230–0.261

Note. θ: potential temperature; σ_0: potential density anomaly; CE1 and CE2: cold eddy 1 and cold eddy 2; CEP1 and CEP2: the edges of CE1 and CE2; DCML: depth of chlorophyll maximum layer.

demonstrating that the Kuroshio intrusion was the major process controlling the humic-like FDOM and CDOM inventories in the upper 100 m of SCS (Figures 5e–5h). However, C1, C2, and CDOM inventories showed negative deviations at the center of cold eddies and positive deviations at the center of warm eddy and the edges of cold eddies, which suggested that mesoscale eddies could modulate regional CDOM and FDOM inventories in the SCS (Figures 5e–5h).

4.2. Impact of Mesoscale Eddies on Chromophoric and Fluorescent Dissolved Organic Matter Dynamics in the Northern South China Sea

In the SCS, some studies focus on the complex biogeochemical responses to mesoscale eddies, such as nutrient delivery, primary production, phytoplankton community structure, and particle export (Chen et al., 2015; Huang et al., 2010; Xiu & Chai, 2011). However, the impact of mesoscale eddies on CDOM and FDOM dynamics in the northern SCS remains unclear. Our results show different patterns of CDOM and FDOM between the stations inside and outside the eddies.

The centers of the two cold eddies exhibited significantly lower potential temperature, higher density, higher maximum Chl *a* concentration, and shallower depth of Chl *a* maximum layer than at the edges of the cold eddies (*t* test, $p < 0.01$; Table 2). Humic-like FDOM in the upper 100 m was higher inside than outside the cold eddies, likely due to a combination of upwelling of humic-rich deep water and elevated biological activity in response to nutrient supplementation inside the cold eddy (Table 2). Integral average humic-like FDOM and CDOM levels in the upper 100 m inside the cold eddies were 16% to 43% and 18% to 30% higher than outside the cold eddies, respectively. The average tryptophan-like fluorescence (C4) inside the cold eddies were similar to or slightly higher than outside the cold eddies in the upper 100 m, indicating that dilution due to inputs of deep water upwelling was almost equal to any production from biological production inside the cold eddies. However, DOM inside the cold eddies had higher HIX and M:C, and lower BIX and $S_{275-295}$, than DOM outside the cold eddies, consistent with elevated levels of humic-like FDOM and upwelled CDOM that has not been extensively photodegraded inside the cold eddies.

The warm eddy southwest of Taiwan showed very similar hydrographic properties to the adjacent Kuroshio water of the WPS, but significantly higher potential temperature, higher salinity, mixed layer, and DCML depth than the edges of the warm eddy and other regions in the SCS without eddies (*t* test, $p < 0.01$; Figures 6a–6c). The CDOM and FDOM profiles in the upper 100 m inside the warm eddy were similar to the adjacent Kuroshio water, both showing significantly lower CDOM and humic-like FDOM abundances, lower M:C, shallower spectral slopes, but a greater depth of the M:C maximum (Figures 6d–6i) than the regions of the SCS without eddies (*t* test, $p < 0.01$). A small vertical gradient of CDOM and FDOM in the upper 100 m of the warm eddy suggested a greater mixed layer depth and lower biological productivity than the SCS no eddy region, indicating that the warm eddy was formed by the intrusion of the Kuroshio Current. Previous studies by physical oceanographers suggest that warm eddies near the Luzon Strait can be separated from the adjacent Kuroshio Current (Jia & Liu, 2004; Zhao, Liang, & Gan, 2016). Our results provide optical data to support this assumption, suggesting that the optical properties of CDOM should be helpful in the study of active marginal sea-open ocean interactions in the Luzon Strait.

4.3. In Situ Production of Bio-refractory Dissolved Organic Matter in the Dark South China Sea and West Philippine Sea

We observed positive and significant relationships between humic-like components (C1 and C2) and AOU in the dark SCS and WPS (Table 3), indicating in situ production of the two humic-like components as organic matter is oxidized in the water column. The C1 production rate per unit of consumed oxygen in the SCS (3.1×10^{-5} RU/(μmol O_2 kg^{-1})) was larger than in the WPS (2.8×10^{-5} RU/(μmol O_2 kg^{-1})), but both were of a similar magnitude to that observed in the open Pacific and Indian Ocean, and some marginal seas

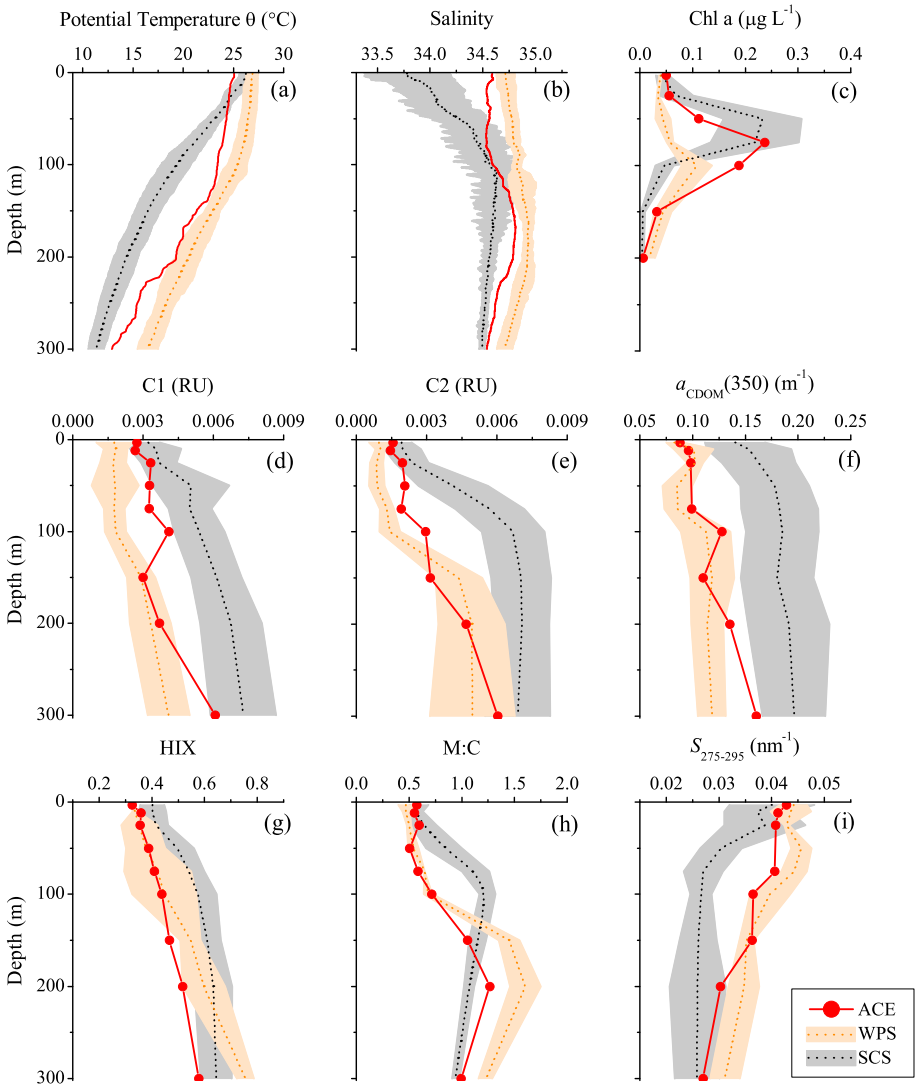

Figure 6. Hydrological and CDOM profiles in the upper 300 m of the warm eddy (ACE, red line and symbol), no eddy region in the northern SCS (the black dotted line means average, and the gray area means standard deviation) and the Kuroshio Current of the WPS (the orange-yellow dotted line means average, and the orange area means standard deviation) in spring 2014.

(e.g., Japan Sea and Okhotsk Sea) (Catalá et al., 2015; Guéguen et al., 2014; Jørgensen et al., 2011; Tanaka et al., 2014; Yamashita et al., 2010, 2007). The C2 production occurred at a much slower rate than C1, with 0.96×10^{-5} RU/(μmol O_2 kg^{-1}) in the SCS and 1.14×10^{-5} RU/(μmol O_2 kg^{-1}) in the WPS. Such a phenomenon was also observed in the dark global ocean, with the production rates of 2.3×10^{-5} RU yr^{-1} for C1 and 1.2×10^{-5} RU yr^{-1} for C2, respectively (Catalá et al., 2015). This might be linked to different complex mechanisms, like hydrological (e.g., age and aging of water mass) and biological factors (e.g., phylogenetic nature of bacteria, archaea, or eukarya) (Catalá et al., 2015; Jørgensen et al., 2011; Tanaka et al., 2014).

M:C vertical profiles in both the tropical SCS and WPS were similar to those in the temperate Okhotsk Sea and the adjacent northwestern Pacific Ocean (Yamashita et al., 2010). However, the maxima in M:C at the bottom of the euphotic layer observed in the northern SCS (~100 m) and the WPS (~200 m) were not reported in the Okhotsk Sea. M:C values at middepths (200–500 m) in the SCS were lower than in the water with the same density in the WPS (Figure 3g). This variation is possibly due to different flux rates and lability of sinking particles between the two regions. Compared to the WPS, SCS has greater primary production, downward and lateral fluxes of particle organic matter (POM) facilitated by the shift of monsoon strength, and frequent occurrence of strong internal waves in the SCS (Alford et al., 2015; Hung et al., 2007; Ma et al., 2017). Therefore, the higher concentration and larger contribution of recently produced POM to the middle water

Table 3
Relationships Between Humic-Like Components (C1 and C2), a_{CDOM} (350) and M:C and AOU in the Dark Ocean of SCS and WPS (>100 m)

Region		C1 (RU)	C2 (RU)	a_{CDOM} (350) (m^{-1})	M:C
SCS	Slope	$(3.09 \pm 0.14) * 10^{-5}$	$(0.96 \pm 0.14) * 10^{-5}$	$(3.26 \pm 0.30) * 10^{-4}$	$(-2.86 \pm 0.08) * 10^{-3}$
	Intercept	$(3.4 \pm 0.22) * 10^{-3}$	$(5.86 \pm 0.23) * 10^{-3}$	0.146 ± 0.005	1.38 ± 0.01
	R^2	0.71	0.19	0.39	0.89
	n	191	190	183	189
	p	<0.01	<0.05	<0.01	<0.01
	F	465.8	44.1	115.0	1454.5
WPS	Slope	$(2.8 \pm 0.31) * 10^{-5}$	$(1.14 \pm 0.29) * 10^{-5}$	$(2.69 \pm 0.39) * 10^{-4}$	$(-4.28 \pm 0.23) * 10^{-3}$
	Intercept	$(2.2 \pm 0.5) * 10^{-3}$	$(4.34 \pm 0.47) * 10^{-3}$	0.107 ± 0.006	1.70 ± 0.04
	R^2	0.72	0.31	0.65	0.92
	n	33	34	27	31
	p	<0.01	<0.05	<0.01	<0.01
	F	81.4	16.0	48.3	356.8

of SCS may have led to greater remineralization and concomitant production of humic-like FDOM, reducing the M:C value compared to the WPS (Figure 3).

Notably, M:C values showed significant negative linear relationships with AOU in the northern SCS and adjacent WPS ($R^2 = 0.89$ and 0.92, $p < 0.001$; Table 3). The intercept of this linear relationship in the SCS (1.38) was lower than in the WPS (1.7), which may be related to the deeper euphotic layer and more photoreactive of C1 compared to C2 in the WPS than in the northern SCS (Yamashita et al., 2010). The slope in the SCS (-2.86×10^{-3}/(μmol O_2 kg^{-1})) was also lower than in the WPS (-4.28×10^{-3}/(μmol O_2 kg^{-1})). Such differences suggest that different mechanisms may occur for carbon storage and accumulation in the deep, aphotic waters of marginal seas versus in the open ocean (Catalá et al., 2015). Future studies of DOM molecular and isotopic character combined with physical and biological studies will be helpful to resolve this issue. The decrease of M:C ratio was accompanied by the increase of HIX value with depth, suggesting that both the M:C and HIX indices are useful indicators of the degree of degradation and the structure of DOM in the dark ocean. This is contrary to the situation in the euphotic layer, where the M:C ratio also reflects the influence of biological production and photodegradation (Coble, 1996; Helms et al., 2013).

The higher production rates in the SCS result in the higher levels of CDOM and FDOM in the SCS intermediate layer water as compared with the WPS. The average levels of C1, C2, C4, and a_{CDOM} (350) between 500 and 1,500 m (corresponding to a potential density from 1026.4 to 1027.4 kg m^{-3}) in the northern SCS was 0.0094 ± 0.0012 RU, 0.0074 ± 0.0010 RU, 0.0031 ± 0.0006 RU and 0.23 ± 0.03 m^{-1}, while the average levels of humic-like C1, C2, and a_{CDOM} (350) in the intermediate water of the WPS, with the same range of potential density, were 0.0076 ± 0.0022 RU, 0.0063 ± 0.0012 RU, 0.0024 ± 0.0006 RU, and 0.16 ± 0.02 m^{-1}. As export from the intermediate layer is the largest outflow of SCS water into the WPS (Tian et al., 2006), the difference in CDOM and FDOM levels between the two water masses will result in the export of "excess" CDOM and FDOM from the marginal seas to the open ocean. The export fluxes of "excess" CDOM and FDOM were estimated based on the difference of average CDOM absorbance and FDOM fluorescence intensity between the northern SCS and the WPS, and the net water flux from the SCS to the WPS through the Luzon Strait (i.e., 5 sverdrup) (Tian et al., 2006). This calculation suggests that the intermediate outflow could export $2.89 \pm 1.70 \times 10^{11}$ RU m^3 yr^{-1} of C1, $1.71 \pm 0.33 \times 10^{11}$ RU m^3 yr^{-1} of C2, $1.12 \pm 0.16 \times 10^{11}$ RU m^3 yr^{-1} of C4, and $1.13 \pm 0.28 \times 10^{13}$ m^2 yr^{-1} of CDOM from the SCS to the Pacific Ocean. Although these estimates have considerable uncertainty, they provide a first estimate of the importance of CDOM and FDOM export from the WPS and SCS to the Pacific Ocean. As these humic-like signatures are preserved in the deep ocean, this delivery may have important implication for carbon sequestration in the global ocean interior (Dai et al., 2009; Catalá et al., 2015).

5. Conclusions

CDOM and FDOM levels in the northern SCS were higher than in the WPS, likely due to higher primary productivity and weaker photodegradation in the euphotic layer and larger particle flux from the surface

into the deep water within the SCS. An isopycnal mixing model indicated that the distributions of humic-like FDOM in the upper northern SCS were dominated by conservative mixing with intrusive Kuroshio water with depleted humic-like components. However, in situ production determined the dynamics of labile protein-like FDOM in the upper 100 m of the northern SCS. Based on the abundance of CDOM and FDOM and reported cross Luzon Strait water fluxes in the intermediate layer (500–1,500 m) from the SCS to the WPS, we estimated that eastward export fluxes of CDOM and FDOM from SCS to the WPS were $2.89 \pm 1.70 \times 10^{11}$ RU m^3 yr^{-1} of C1, $1.71 \pm 0.33 \times 10^{11}$ RU m^3 yr^{-1} of C2, $1.12 \pm 0.16 \times 10^{11}$ RU m^3 yr^{-1} of C4, and $1.13 \pm 0.28 \times 10^{13}$ m^2 yr^{-1} of CDOM. These results highlight the considerable role of the SCS in the global ocean carbon reserve.

DOM inside a warm eddy in the northeastern SCS had similar optical properties to the Kuroshio water from which it was apparently formed, providing optical evidence that warm eddies do indeed separate from the Kuroshio Current through the Luzon Strait. DOM in two cold eddies exhibited higher CDOM and FDOM levels, higher HIX and M:C, and shallower spectral slope than DOM at the edges of the cold eddies and other eddy-free regions in the northern SCS. The elevated levels of CDOM and FDOM in the cold eddies is likely explained by the upwelling of CDOM-rich and FDOM-rich deep water and enhanced primary productivity inside the cold eddy. Further studies are needed to examine the seasonal variation of the Kuroshio intrusion and its impact upon DOM dynamics and also to understand the complex mechanisms involved in the response of DOM dynamics to mesoscale processes.

Acknowledgments

Data supporting this study are available in the supporting information data set. This work was financially supported by the National Natural Science Foundation of China (NSFC) (41276064), the Joint Fund Program for Promoting S&T Cooperation Across the Taiwan Straits supported by NSFC and Fujian Province (U1305231), and the Senior User Project of R/V *KEXUE* (KEXUE2017G11). We thank the caption, crew, and scientists aboard the R/V *Shiyan III*, led by chief scientist Huabin Mao, for their support during the cruise. Special thanks are given to Jian Ma, Jing Xu, Jia Wei, and Ye Xu for their help in sampling, analysis, and data processing. John Hodgkiss and Stephan Steinke are thanked for their comments and assistances with English. We would also like to thank the two anonymous reviewers for their valuable comments and suggestions.

References

Alford, M. H., Peacock, T., MacKinnon, J. A., Nash, J. D., Buijsman, M. C., Centuroni, L. R., … (David) Tang, T. Y. (2015). The formation and fate of internal waves in the South China Sea. *Nature*, *521*(7550), 65–69. https://doi.org/10.1038/nature14399

Carpenter, J. H. (1965). The Chesapeake Bay Institute technique for the Winkler dissolved oxygen method. *Limnology and Oceanography*, *10*(1), 141–143. https://doi.org/10.4319/lo.1965.10.1.0141

Catalá, T. S., Reche, I., Fuentes-Lema, A., Romera-Castillo, C., Nieto-Cid, M., Ortega-Retuerta, E., … Álvarez-Salgado, X. A. (2015). Turnover time of fluorescent dissolved organic matter in the dark global ocean. *Nature Communications*, *6*, 5986. https://doi.org/10.1038/ncomms6986

Chao, S. Y., Shaw, P. T., & Wang, J. (1995). Wind relaxation as possible cause of the South China Sea Warm Current. *Journal of Oceanography*, *51*(1), 111–132. https://doi.org/10.1007/BF02235940

Chen, Y.-L. L., Chen, H.-Y., Jan, S., Lin, Y.-H., Kuo, T.-H., & Hung, J.-J. (2015). Biologically active warm-core anticyclonic eddies in the marginal seas of the western Pacific Ocean. *Deep Sea Research, Part I*, *106*, 68–84. https://doi.org/10.1016/j.dsr.2015.10.006

Chen, Y.-L. L., Chen, H.-Y., Lin, I. I., Lee, M.-A., & Chang, J. (2007). Effects of cold eddy on phytoplankton production and assemblages in Luzon Strait bordering the South China Sea. *Journal of Oceanography*, *63*(4), 671–683. https://doi.org/10.1007/s10872-007-0059-9

Chen, C. T. A., Wang, S. L., Wang, B. J., & Pai, S. C. (2001). Nutrient budgets for the South China Sea basin. *Marine Chemistry*, *75*(4), 281–300. https://doi.org/10.1016/s0304-4203(01)00041-x

Coble, P. G. (1996). Characterization of marine and terrestrial DOM in seawater using excitation emission matrix spectroscopy. *Marine Chemistry*, *51*(4), 325–346. https://doi.org/10.1016/0304-4203(95)000623

Coble, P. G. (2007). Marine optical biogeochemistry: The chemistry of ocean color. *Chemical Reviews*, *107*(2), 402–418. https://doi.org/10.1021/cr050350+

Coble, P. G., Del Castillo, C. E., & Avril, B. (1998). Distribution and optical properties of CDOM in the Arabian Sea during the 1995 Southwest Monsoon. *Deep Sea Research Part II: Topical Studies in Oceanography*, *45*(10-11), 2195–2223. https://doi.org/10.1016/s0967-0645(98)00068-x

Coble, P. G., Lead, J., Baker, A., Reynolds, D. M., & Spencer, R. G. M. (2014). *Aquatic organic matter fluorescence*, *Cambridge Environmental Chemistry Series* (pp. 313–314). Cambridge, UK: Cambridge University Press. https://doi.org/10.1017/CBO9781139045452

Conmy, R. N., Coble, P. G., Cannizzaro, J. P., & Heil, C. A. (2009). Influence of extreme storm events on West Florida Shelf CDOM distributions. *Journal of Geophysical Research*, *114*, G00F04. https://doi.org/10.1029/2009JG000981

Dai, M., Cao, Z., Guo, X., Zhai, W., Liu, Z., Yin, Z., … Du, C. (2013). Why are some marginal seas sources of atmospheric CO_2? *Geophysical Research Letters*, *40*(10), 2154–2158. https://doi.org/10.1002/grl.50390

Dai, M., Meng, F., Tang, T., Kao, S.-J., Lin, J., Chen, J., … Yang, S. (2009). Excess total organic carbon in the intermediate water of the South China Sea and its export to the North Pacific. *Geochemistry, Geophysics, Geosystems*, *10*, Q12002. https://doi.org/10.1029/2009GC002752

D'Sa, E. J., Steward, R. G., Vodacek, A., Blough, N. V., & Phinney, D. (1999). Determining optical absorption of colored dissolved organic matter in seawater with a liquid capillary waveguide. *Limnology and Oceanography*, *44*(4), 1142–1148. https://doi.org/10.4319/lo.1999.44.4.1142

Du, C., Liu, Z., Dai, M., Kao, S. J., Cao, Z., Zhang, Y., … Li, Y. (2013). Impact of the Kuroshio intrusion on the nutrient inventory in the upper northern South China Sea: Insights from an isopycnal mixing model. *Biogeosciences*, *10*(10), 6419–6432. https://doi.org/10.5194/bg-10-6419-2013

Fichot, C. G., & Benner, R. (2011). A novel method to estimate DOC concentrations from CDOM absorption coefficients in coastal waters. *Geophysical Research Letters*, *38*, L03610. https://doi.org/10.1029/2010GL046152

Floge, S. A., Hardy, K. R., Boss, E., & Wells, M. L. (2009). Analytical intercomparison between type I and type II long-pathlength liquid core waveguides for the measurement of chromophoric dissolved organic matter. *Limnology and Oceanography: Methods*, *7*(4), 260–268. https://doi.org/10.4319/lom.2009.7.260

Guéguen, C., Cuss, C. W., Cassels, C. J., & Carmack, E. C. (2014). Absorption and fluorescence of dissolved organic matter in the waters of the Canadian Arctic Archipelago, Baffin Bay, and the Labrador Sea. *Journal of Geophysical Research: Oceans*, *119*, 2034–2047. https://doi.org/10.1002/2013JC009173

Guo, W., Yang, L., Hong, H., Stedmon, C. A., Wang, F., Xu, J., & Xie, Y. (2011). Assessing the dynamics of chromophoric dissolved organic matter in a subtropical estuary using parallel factor analysis. *Marine Chemistry*, *124*(1-4), 125–133. https://doi.org/10.1016/j.marchem.2011.01.003

Guo, W., Yang, L., Zhai, W., Chen, W., Osburn, C. L., Huang, X., & Li, Y. (2014). Runoff-mediated seasonal oscillation in the dynamics of dissolved organic matter in different branches of a large bifurcated estuary: The Changjiang Estuary. *Journal of Geophysical Research: Biogeosciences*, *119*, 776–793. https://doi.org/10.1002/2013JG002540

Hansen, A. M., Kraus, T. E. C., Pellerin, B. A., Fleck, J. A., Downing, B. D., & Bergamaschi, B. A. (2016). Optical properties of dissolved organic matter (DOM): Effects of biological and photolytic degradation. *Limnology and Oceanography*, *61*(3), 1015–1032. https://doi.org/10.1002/lno.10270

Helms, J. R., Stubbins, A., Perdue, E. M., Green, N. W., Chen, H., & Mopper, K. (2013). Photochemical bleaching of oceanic dissolved organic matter and its effect on absorption spectral slope and fluorescence. *Marine Chemistry*, *155*, 81–91. https://doi.org/10.1016/j.marchem.2013.05.015

Helms, J. R., Stubbins, A., Ritchie, J. D., Minor, E. C., Kieber, D. J., & Mopper, K. (2008). Absorption spectral slopes and slope ratios as indicators of molecular weight, source, and photobleaching of chromophoric dissolved organic matter. *Limnology and Oceanography*, *53*(3), 955–969. https://doi.org/10.4319/lo.2008.53.3.0955

Huang, B., Hu, J., Xu, H., Cao, Z., & Wang, D. (2010). Phytoplankton community at warm eddies in the northern South China Sea in winter 2003/2004. *Deep Sea Research Part II: Topical Studies in Oceanography*, *57*(19-20), 1792–1798. https://doi.org/10.1016/j.dsr2.2010.04.005

Hung, J. J., Wang, S. M., & Chen, Y. L. (2007). Biogeochemical controls on distributions and fluxes of dissolved and particulate organic carbon in the northern south china sea. *Deep Sea Research Part II Topical Studies in Oceanography*, *54*(14–15), 1486–1503. https://doi.org/10.1016/j.dsr2.2007.05.006

Huguet, A., Vacher, L., Relexans, S., Saubusse, S., Froidefond, J. M., & Parlanti, E. (2009). Properties of fluorescent dissolved organic matter in the Gironde Estuary. *Organic Geochemistry*, *40*(6), 706–719. https://doi.org/10.1016/j.orggeochem.2009.03.002

Jia, Y. L., & Liu, Q. Y. (2004). Eddy shedding from the Kuroshio bend at Luzon Strait. *Journal of Oceanography*, *60*(6), 1063–1069. https://doi.org/10.1007/s10872-005-0014-6

Jørgensen, L., Stedmon, C. A., Kragh, T., Markager, S., Middelboe, M., & Søndergaard, M. (2011). Global trends in the fluorescence characteristics and distribution of marine dissolved organic matter. *Marine Chemistry*, *126*(1-4), 139–148. https://doi.org/10.1016/j.marchem.2011.05.002

Kitidis, V., Stubbins, A. P., Uher, G., Goddard, R. C. U., Law, C. S., & Woodward, E. M. S. (2006). Variability of chromophoric organic matter in surface waters of the Atlantic Ocean. *Deep Sea Research Part II: Topical Studies in Oceanography*, *53*(14-16), 1666–1684. https://doi.org/10.1016/j.dsr2.2006.05.009

Kowalczuk, P., Tilstone, G. H., Zablocka, M., Rottgers, R., & Thomas, R. (2013). Composition of dissolved organic matter along an Atlantic meridional transect from fluorescence spectroscopy and parallel factor analysis. *Marine Chemistry*, *157*, 170–184. https://doi.org/10.1016/j.marchem.2013.10.00

Lakowicz, J. R. (2006). *Principles of Fluorescence Spectroscopy* (pp. 623–674). New York: Springer. https://doi.org/10.1007/978-0-387-46312-4_19

Lawaetz, A. J., & Stedmon, C. A. (2009). Fluorescence intensity calibration using the Raman scatter peak of water. *Applied Spectroscopy*, *63*(8), 936–940. https://doi.org/10.1366/000370209788964548

Li, L., Nowlin, W. D., & Jilan, S. (1998). Anticyclonic rings from the Kuroshio in the South China Sea. *Deep Sea Research Part I: Oceanographic Research Papers*, *45*(9), 1469–1482. https://doi.org/10.1016/s0967-0637(98)00026-0

Lin, I. I., Lien, C.-C., Wu, C.-R., Wong, G. T. F., Huang, C.-W., & Chiang, T.-L. (2010). Enhanced primary production in the oligotrophic South China Sea by eddy injection in spring. *Geophysical Research Letters*, *37*, L16602. https://doi.org/10.1029/2010GL043872

Loginova, A. N., Thomsen, S., & Engel, A. (2016). Chromophoric and fluorescent dissolved organic matter in and above the oxygen minimum zone off Peru. *Journal of Geophysical Research: Oceans*, *121*, 7973–7990. https://doi.org/10.1002/2016JC011906

Lorenzoni, L., Hu, C., Varela, R., Arias, G., Guzmán, L., & Muller-Karger, F. (2011). Bio-optical characteristics of cariaco basin (caribbean sea) waters. *Continental Shelf Research*, *31*(6), 582–593. https://doi.org/10.1016/j.csr.2010.12.013

Ma, H., Yang, W., Zhang, L., Zhang, R., Chen, M., Qiu, Y., & Zheng, M. (2017). Utilizing 210Po deficit to constrain particle dynamics in mesopelagic water, western South China Sea. *Geochemistry, Geophysics, Geosystems*, *18*(4), 1594–1607. https://doi.org/10.1002/2017GC006899

McGillicuddy, D. J. Jr. (2016). Mechanisms of physical-biological-biogeochemical interaction at the oceanic mesoscale. *Annual Review of Marine Science*, *8*(1), 125–159. https://doi.org/10.1146/annurev-marine-010814-015606

McGillicuddy, D. J. Jr., Robinson, A. R., Siegel, D. A., Jannasch, H. W., Johnson, R., Dickeys, T., … Knap, A. H. (1998). Influence of mesoscale eddies on new production in the Sargasso Sea. *Nature*, *394*(6690), 263–266. https://doi.org/10.1038/28367

Miller, R. L., Belz, M., Del Castillo, C., & Trzaska, R. (2002). Determining CDOM absorption spectra in diverse coastal environments using a multiple pathlength, liquid core waveguide system. *Continental Shelf Research*, *22*(9), 1301–1310. https://doi.org/10.1016/s0278-4343(02)00009-2

Mopper, K., Kieber, D. J., & Stubbins, A. (2015). Marine photochemistry of organic matter: Processes and impacts. In D. A. Hansell & C. A. Carlson (Eds.), *Biogeochemistry of marine dissolved organic matter* (2nd ed., pp. 389–450). New York: Elsevier. https://doi.org/10.1016/B978-0-12-405940-5.00008-X

Moran, M. A., Sheldon, W. M., & Zepp, R. G. (2000). Carbon loss and optical property changes during long-term photochemical and biological degradation of estuarine dissolved organic matter. *Limnology and Oceanography*, *45*(6), 1254–1264. https://doi.org/10.4319/lo.2000.45.6.1254

Nelson, N. B., & Siegel, D. A. (2013). The global distribution and dynamics of chromophoric dissolved organic matter. *Annual Review of Marine Science*, *5*(1), 447–476. https://doi.org/10.1146/annurev-marine-120710-100751

Nelson, N. B., Siegel, D. A., Carlson, C. A., & Swan, C. M. (2010). Tracing global biogeochemical cycles and meridional overturning circulation using chromophoric dissolved organic matter. *Geophysical Research Letters*, *37*, L03610. https://doi.org/10.1029/2009GL042325

Nelson, N. B., Siegel, D. A., Carlson, C. A., Swan, C., Smethie, W. M., & Khatiwala, S. (2007). Hydrography of chromophoric dissolved organic matter in the North Atlantic. *Deep Sea Research Part I: Oceanographic Research Papers*, *54*(5), 710–731. https://doi.org/10.1016/j.dsr.2007.02.006

Nelson, N. B., Siegel, D. A., & Michaels, A. F. (1998). Seasonal dynamics of colored dissolved material in the Sargasso Sea. *Deep Sea Research Part I: Oceanographic Research Papers*, *45*(6), 931–957. https://doi.org/10.1016/s0967-0637(97)00106-4

Ohno, T. (2002). Fluorescence inner-filtering correction for determining the humification index of dissolved organic matter. *Environmental Science & Technology*, *36*(4), 742–746. https://doi.org/10.1021/es0155276

Qu, T., Mitsudera, H., & Yamagata, T. (2000). Intrusion of the North Pacific waters into the South China Sea. *Journal of Geophysical Research, Oceans*, *105*(C3), 6415–6424. https://doi.org/10.1029/1999JC900323

Siegel, D. A., Maritorena, S., Nelson, N. B., Hansell, D. A., & Lorenzi-Kayser, M. (2002). Global distribution and dynamics of colored dissolved and detrital organic materials. *Journal of Geophysical Research*, *107*(C12), 3228. https://doi.org/10.1029/2001JC000965

Spencer, R. G. M., & Coble, P. G. (2014). Sampling design for organic matter fluorescence analysis. In P. G. Coble, et al. (Eds.), *Aquatic organic matter fluorescence* (pp. 125–146). Cambridge: Cambridge University Press.

Stedmon, C. A., & Bro, R. (2008). Characterizing dissolved organic matter fluorescence with parallel factor analysis: A tutorial. *Limnology and Oceanography: Methods*, *6*(11), 572–579. https://doi.org/10.4319/lom.2008.6.572

Stedmon, C. A., & Markager, S. (2005). Resolving the variability in dissolved organic matter fluorescence in a temperate estuary and its catchment using PARAFAC analysis. *Limnology and Oceanography*, *50*(2), 686–697. https://doi.org/10.4319/lo.2005.50.2.0686

Stedmon, C. A., Markager, S., & Bro, R. (2003). Tracing dissolved organic matter in aquatic environments using a new approach to fluorescence spectroscopy. *Marine Chemistry*, *82*(3-4), 239–254. https://doi.org/10.1016/s0304-4203(03)00072-0

Stubbins, A., Uher, G., Law, C. S., Mopper, K., Robinson, C., & Upstill-Goddard, R. C. (2006). Open-ocean carbon monoxide photoproduction. *Deep Sea Research Part II: Topical Studies in Oceanography*, *53*(14-16), 1695–1705. https://doi.org/10.1016/j.dsr2.2006.05.011

Swan, C. M., Siegel, D. A., Nelson, N. B., Carlson, C. A., & Nasir, E. (2009). Biogeochemical and hydrographic controls on chromophoric dissolved organic matter distribution in the Pacific Ocean. *Deep Sea Research Part I: Oceanographic Research Papers*, *56*(12), 2175–2192. https://doi.org/10.1016/j.dsr.2009.09.002

Tanaka, K., Kuma, K., Hamasaki, K., & Yamashita, Y. (2014). Accumulation of humic-like fluorescent dissolved organic matter in the Japan Sea. *Scientific Reports*, *4*(1). https://doi.org/10.1038/srep05292

Tian, J., Yang, Q., Liang, X., Xie, L., Hu, D., Wang, F., & Qu, T. (2006). Observation of Luzon Strait transport. *Geophysical Research Letters*, *33*, L1967. https://doi.org/10.1029/2006GL026272

Tseng, C. M., Wong, G. T. F., Chou, W. C., Lee, B. S., Sheu, D. D., & Liu, K. K. (2007). Temporal variations in the carbonate system in the upper layer at the seats station. *Deep Sea Research Part II: Topical Studies in Oceanography*, *54*(14-15), 1448–1468. https://doi.org/10.1016/j.dsr2.2007.05.003

Wong, G. T. F., Ku, T.-L., Mulholland, M., Tseng, C.-M., & Wang, D.-P. (2007). The South East Asian Time-series Study (SEATS) and the biogeochemistry of the South China Sea—An overview. *Deep Sea Research Part II: Topical Studies in Oceanography*, *54*(14-15), 1434–1447. https://doi.org/10.1016/j.dsr2.2007.05.012

Wu, K., Dai, M., Chen, J., Meng, F., Li, X., Liu, Z., … Gan, J. (2015). Dissolved organic carbon in the South China Sea and its exchange with the Western Pacific Ocean. *Deep Sea Research Part II: Topical Studies in Oceanography*, *122*, 41–51. https://doi.org/10.1016/j.dsr2.2015.06.013

Wyrtki, K. (1961). Physical oceanography of the southeast Asian waters, Naga Rep. 2, 195 pp., Scripps Inst. of Oceanogr., La Jolla, CA.

Xiu, P., & Chai, F. (2011). Modeled biogeochemical responses to mesoscale eddies in the South China Sea. *Journal of Geophysical Research: Oceans*, *116*, C10006. https://doi.org/10.1029/2010JC006800

Xiu, P., Chai, F., Shi, L., Xue, H., & Chao, Y. (2010). A census of eddy activities in the South China Sea during 1993-2007. *Journal of Geophysical Research*, *115*, C03012. https://doi.org/10.1029/2009JC005657

Xue, H. J., Chai, F., Pettigrew, N., Xu, D. Y., Shi, M., & Xu, J. P. (2004). Kuroshio intrusion and the circulation in the South China Sea. *Journal of Geophysical Research*, *109*, C02017. https://doi.org/10.1029/2002JC001724

Yamashita, Y., Cory, R. M., Nishioka, J., Kuma, K., Tanoue, E., & Jaffé, R. (2010). Fluorescence characteristics of dissolved organic matter in the deep waters of the Okhotsk Sea and the northwestern North Pacific Ocean. *Deep Sea Research Part II: Topical Studies in Oceanography*, *57*(16), 1478–1485. https://doi.org/10.1016/j.dsr2.2010.02.016

Yamashita, Y., & Tanoue, E. (2008). Production of bio-refractory fluorescent dissolved organic matter in the ocean interior. *Nature Geoscience*, *1*(9), 579–582. https://doi.org/10.1038/ngeo279

Yamashita, Y., Tsukasaki, A., Nishida, T., & Tanoue, E. (2007). Vertical and horizontal distribution of fluorescent dissolved organic matter in the Southern Ocean. *Marine Chemistry*, *106*(3-4), 498–509. https://doi.org/10.1016/j.marchem.2007.05.004

Zhang, Y., Sintes, E., Chen, M., Zhang, Y., Dai, M., Jiao, N., & Herndl, G. J. (2009). Role of mesoscale cyclonic eddies in the distribution and activity of archaea and bacteria in the South China Sea. *Aquatic Microbial Ecology*, *56*, 65–79. https://doi.org/10.3354/ame01324

Zhao, Y. B., Liang, X. S., & Gan, J. (2016). Nonlinear multiscale interactions and internal dynamics underlying a typical eddy-shedding event at Luzon Strait. *Journal of Geophysical Research: Oceans*, *121*, 8208–8229. https://doi.org/10.1002/2016JC012483

Zhou, K., Dai, M., Kao, S.-J., Wang, L., Xiu, P., Chai, F., … Liu, Y. (2013). Apparent enhancement of Th-234-based particle export associated with anticyclonic eddies. *Earth and Planetary Science Letters*, *381*, 198–209. https://doi.org/10.1016/j.epsl.2013.07.039